Spring 2021

Lions, Tigers, and Hemes - Oh My! A Dynamic Look at the Electronic Effects of Porphyrin Substitution on Cytochrome P450 OleT

Alexis J. Holwerda
University of South Carolina - Columbia

LIONS, TIGERS, AND HEMES - OH MY! A DYNAMIC LOOK AT THE ELECTRONIC EFFECTS OF PORPHYRIN SUBSTITUTION ON CYTOCHROME P450 OLET

By

Alexis J. Holwerda

Submitted in Partial Fulfillment
of the Requirements for
Graduation with Honors from the
South Carolina Honors College

May 2021

Approved:

Dr. Thomas Makris
Director of Thesis

Dr. Maksymilian Chruszcz
Second Reader

Steve Lynn, Dean

For South Carolina Honors College

ACKNOWLEDGEMENTS

First, I would like to thank my advisor, Dr. Makris, for the opportunity to research in his lab. The knowledge I have gained under his mentorship over the past three years is unquantifiable. I am incredibly grateful for the passion and skills instilled in me that I will be able to carry into my future endeavors.

I would like to thank my second reader, Dr. Chruszcz, for his time and guidance over the past year – both through the thesis process and in research. I am grateful for the opportunity to join his lab and would like to thank all of the members of the Chruszcz Lab for their support over the last year.

Next, I would like to thank all of the members of the Makris Lab team. Their support and lab dynamic throughout the thesis process, and over my time as an undergraduate in the lab, has made my time at UofSC special. This project could not have been completed without them. I would like to give a special thank you to Olivia Manley for her support throughout my thesis.

Finally, I would like to thank my family and friends for their support and love over my life. I would especially like to thank my parents for their unending kindness and support from day one, I would not be where I am without them, and their support.

ABSTRACT

OleT, a member of the CYP152 family of cytochrome P450s (CYPs), decarboxylates fatty acids using hydrogen peroxide as an oxidant. The resultant products are a terminal alkene and carbon dioxide. This C–C cleavage reaction is highly atypical for CYPs, which prototypically oxygenate substrates, and provides a potential means to enzymatically produce drop-in fuels. OleT contains a heme-iron cofactor that facilitates decarboxylation through the activation of hydrogen peroxide. The catalytic cycle, as determined by transient kinetics, includes two ferryl intermediates known as Compound I (Ole-I) and Compound II (Ole-II). Ole-I performs substrate hydrogen abstraction and subsequent single electron transfer to Ole-II induces C–C bond cleavage. Previous studies of OleT orthologs have demonstrated that chemoselectivity of the enzyme is reinforced, in part, from exquisite binding of fatty acids within the distal substrate-binding pocket. However, it has remained unclear how ground-state thermodynamics may also influence OleT ferryl reactivity. This research probes the impact of heme-electronics on the intermediates of OleT catalysis through the substitution of native iron-protoporphyrin IX with an iron-mesoporphyrin, which replaces the heme-vinyl groups with ethyl substituents, and iron-deuteroporphyrin IX, which replaces the heme-vinyl groups with hydrogen substituents, both of which alter the redox potential of the iron. Transient kinetic studies at variable temperatures have been used to measure the direct impact of this alteration on C–H abstraction barriers. Analysis of the Eyring plots has been used to provide the first full thermodynamic description of Compound I reactivity, revealing the importance of entropic factors in modulating the process. These results suggest a strong linkage between heme electronics and the metabolic efficiency of OleT and offer a strategy for modulating the reactivity of this ubiquitously distributed superfamily of enzymes.

TABLE OF CONTENTS

INTRODUCTION

Recently, the need for alternative fuel sources has become significant to the research community due to a decrease in resources and growing environmental impact[1]. Great attention has been given to the production of fuels from biological sources (i.e., biofuels) as a less environmentally taxing alternative to harvesting crude oil. “Drop-in” biofuels, or those that are compatible with the existing transportation machinery, have come to the forefront of research, and a number of mechanisms for production have been promising[1]. Several metalloenzymes, including OleT, have been recognized as targets for manipulating cellular machinery for alkene synthesis from fatty acids (FAs)[2].

A member of the cytochrome P450 (CYP) superfamily of proteins, OleT has been identified for its olefin synthesis in Jeotgalicoccus sp.[3] Specifically, OleT is a member of the CYP152 family, which is categorized by their utilization of hydrogen peroxide as the native oxidant, as opposed to dioxygen[4]. OleT contains a heme center, which is an integral aspect to the iron-assisted catalysis. The catalytic mechanism for OleT proceeds through the reaction of the ferric high-spin iron with H_2O_2 to generate two intermediates, Compound I, an iron (IV)-oxo species (shown as 3 in Scheme 1), and Compound II, an iron (IV)-OH species (4), which are both spectroscopically visible and distinguishable using transient rapid-mix stopped-flow spectroscopy.[5, 6]. OleT metabolism of FAs relies on C–H abstraction from the C3 position by Compound I (Ole-I) to generate a substrate radical and Compound-II (Ole-II). This step is followed by oxidative C–C scission induced by proton-coupled electron transfer to Compound II to form carbon dioxide and the alkene product,[6] ultimately restoring the ferric-aquo resting state of the enzyme.

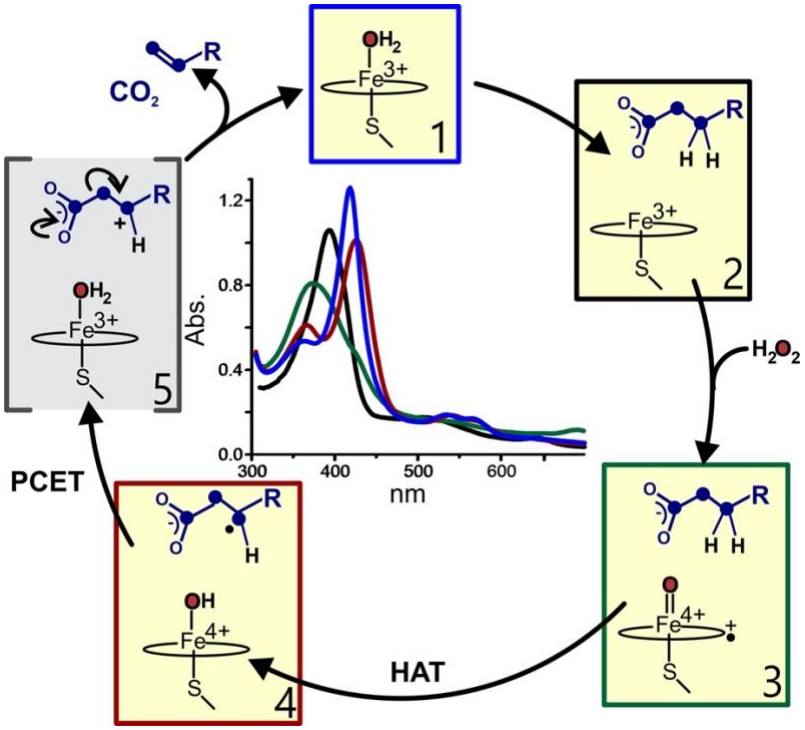

Scheme 1: Overall catalytic cycle, and accompanying optical spectra, of the OleT oxidative decarboxylation of fatty acids to terminal alkenes and CO_2. The low-spin ferric-aquo resting state (1, blue) converts to the substrate-bound high-spin form (2, black). Peroxide activation forms the iron(IV)-oxo π-cation radical Compound I (3, green), and C-H hydrogen atom transfer (HAT) yields the iron(IV)-hydroxo Compound II (4, red). A proton-coupled electron transfer (PCET) step regenerates the low-spin ferric-aquo state and initiates decarboxylation of the fatty acid substrate (5, grey); however, this has not been directly observed.

Research on OleT tends to focus on increasing turnover efficiency, as this enhances its potential as an economically desirable fuel alternative. Past studies have included identification of hydrogen peroxide as a co-substrate[3, 7], pairing OleT with a continuous hydrogen peroxide supply to improve efficiency[8], as well as creating a multi-enzyme assembly to increase the substrate binding ability of OleT[9]. Another potential method to affect OleT efficiency is to tune the heme center, thus changing the redox potential, or the ability to activate hydrogen peroxide.

Until this point, it has remained unclear how ground-state thermodynamics affect the reactivity of Ole-I and Ole-II. In determining the driving factors behind C-H bond activation, ground-state thermodynamics must be separated from other factors in order to determine which has a dominant role in lowering the activation barrier. Thermodynamic parameters, such as redox potential, of other proteins in the cytochrome family have been reported [10-12]; however, the CYP family is diverse in its redox partner system, and the parameters determined for one enzyme class may not be applicable for another enzyme class[12]. A recent study[13] estimated the redox potentials of Compound-I and Compound-II as $E^{o\prime}_{Cpd-I} \sim 1.2\,V$ and $E^{o\prime}_{Cpd-II} \sim 0.9\,V$ in CYP158, another cytochrome P450 enzyme. Unlike OleT, CYP158 is an oxygen activating cytochrome, so the reduction potentials may differ from those observed for OleT, which utilizes peroxide as a co-substrate[14]. There appears to be a wide range of redox potentials in the cytochrome family, thus this study aims to provide more data about the expected thermodynamic values. In addition, the linkage of resting-state redox parameters on ferryl reactivity have yet to be interrogated.

In order to explore the thermodynamics of OleT, heme cofactor substitution of the native protoporphyrin IX has been employed to alter redox properties without altering other elements of the protein that may contribute to catalysis, notably the heme distal pocket and axial thiolate ligand. Heme cofactor substitution has been shown to alter redox potentials and other thermodynamic parameters in other heme-cofactor dependent enzymes, such as thiolate-ligated NO synthases (NOS)[15] and histidine-ligated myoglobin[16, 17] and horseradish peroxidase[16]. In NOS enzymes in particular, mesoporphyrin IX (Scheme 2) substitution lowered redox potentials, as mesoporphyrin has less pi-electron conjugation and is a more electron-rich porphyrin ring compared to protoporphyin[15], and so a similar result was expected for OleT. Deuteroporphyrin IX (Scheme 2)

was likely to also lower the redox potential of OleT, due to being similarly more electron-rich, however literature does not provide a clear precedence for this.

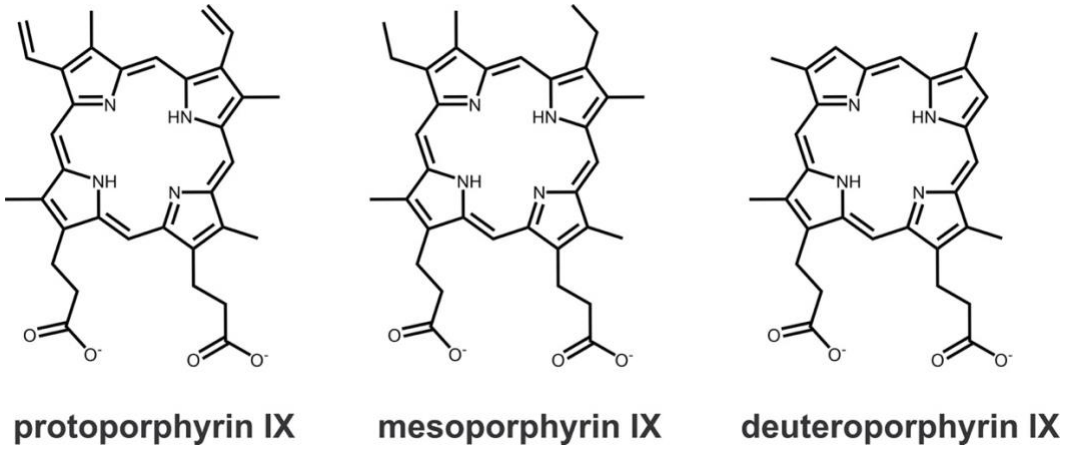

Scheme 2: The native porphyrin, protoporphyrin IX, and the substituted porphyrins employed in this study. *In vivo,* all three porphyrins will form an iron-porphyrin complex.

The goal of this work was to directly investigate the full thermodynamic parameters contributing to Compound I and II reactivity in Cytochrome P450s. Due to the spectroscopically-active nature of the system, direct measurement of activation barriers, in conjunction with electropotential measurements, provides a clearer view into the reactivity as compared to previous work based solely on reduction potentials or density functional theory[13, 18-20]. This involved growth and purification of heme-substituted cytochrome P450 OleT, which was then characterized using a variety of biophysical methods. Utilizing kinetics, the direct linkage of ground-state thermodynamic influence on the reactivity of P450 Compound I are reported.

MATERIALS AND METHODS

Reagents

Microbiology reagents and media were purchased from Research Products International. Antibiotics and isopropyl- β-d-thiogalactopyranoside (IPTG) were purchased from Gold Biotechnology. Buffers and chloramphenicol were purchased from VWR International. Methyl viologen, Safranin T, Neutral Red, and sodium hydrosulfite were purchased from Sigma-Aldrich. Fe-mesoporphyrin IX and Fe-deuteroporphyrin IX were purchased from Frontier Scientific.

Expression and Purification

Native Fe-protoporphyrin IX containing $OleT_{JE}$ (OleT-PP) was expressed and purified following previously published procedures[21]. Fe-mesoporphyrin IX and Fe-deuteroporphyrin IX reconstituted $OleT_{JE}$ (OleT-MP and OleT-DP, respectively) were coexpressed with heme importer ChuA (pChuA), and GroES/GroEL/Tig chaperones. A transformation was performed following standard protocols[22] to insert ChuA and $OleT_{JE}$ plasmids into BL-21 (DE3) competent *E. coli* cells. Colonies from the transformation were incubated overnight in 120 mL Luria Broth cultures at 37 °C while shaking with ampicillin (50 μg/L), kanamycin (50 μg/L), and chloramphenicol (35 μg/L) added.

The 120 mL cultures were used to inoculate large scale (1 L) growths in modified M9 minimal media supplemented with: 0.4% glucose, 10 g/L casamino acids, 2 mM $MgSO_4$, and. 0.1 mM $CaCl_2$. The antibiotics ampicillin (50 μg/L), kanamycin (50 μg/L), and chloramphenicol (35 μg/L) were also added in order to select for ChuA, OleT, and the chaperones. Cultures were placed in a shaker at 37 °C and 200 rpm. Once an OD_{600nm} between 1.0 and 1.5 was reached, the culture temperature was lowered from 37 °C to 18 °C and tetracycline (10 μg/L), IPTG (50 μM), and Fe-

mesoporphyrin IX (2 μM) or Fe-deuteroporphyrin IX (2 μM) were added. Cells were allowed to incubate and were harvested after 24 hours. The purification protocol followed that of OleT-PP.

Heme Incorporation Confirmation

Heme incorporation was verified in two ways. Following purification, optical spectroscopy was used to observe Soret maxima shifts relative to that of OleT-PP, consistent with shifts reported for other heme enzymes[15, 23]. Based on studies done with $P450_{cam,}$ blue-shifts of around 13 nm and 8 nm were expected for MP and DP as compared to the native PP, respectively[23]. Then, heme incorporation was further confirmed using analysis by liquid chromatography-mass spectrometry. The heme was extracted[24] from each isolated protein (OleT-MP and OleT-DP) and compared to standards of Fe-mesoporphyrin IX, Fe-deuteroporphyrin IX, or Fe-protoporphyrin IX. The incorporation of the non-native porphyrin was determined to be >90% in all cases.

Optical Spectroscopy

Optical spectra were recorded utilizing an Agilent/HP 8453 UV-Vis spectrophotometer. Optical characterizations were performed using 6-10 μM protein in 200 mM K_2HPO_4 (pH 7.5).

Fatty Acid Binding Titrations

Binding titrations were performed using 6-10 μM protein in 200 mM K_2HPO_4 (pH 7.5). A 10 mM eicosanoic acid (EA) stock dissolved in 70% ethanol:30% Triton X-100 was used for substrate binding. OleT was prepared substrate-free through the addition of excess H_2O_2 to turnover bound fatty acids and desalting. Desalting was done by loading the protein onto a PD-10 desalting column and eluting with 200 mM K_2HPO_4 (pH 7.5). Fatty acid substrate titrations were

performed by sequentially adding EA to substrate free protein and monitoring absorbance changes. The absorbance was monitored at A_{obs} = 417 nm and 395 nm for OleT-PP, and absorbance changes were fit to a Morrison equation using Origin software[5, 6]. Monitoring absorbances at 417 nm and 395 nm provides a quantitative measurement of the transition from the low- to high-spin conformation. This method was identical for OleT-MP, however A_{obs} = 408 nm and 382 nm, and for OleT-DP A_{obs} = 410 nm and 387 nm. The monitored wavelength shift was necessitated by the spectral shifts that resulted from heme substitution.

The CO-bound complex was prepared using dithionite solutions that were prepared in septa-sealed vials. The dithionite solution concentration was determined via optical spectroscopy in a sealed anaerobic cuvette prior to use with ε_{315} = 8 mM^{-1} cm^{-1}. Oxygen-free EA-bound OleT was prepared in septa-sealed vials and degassed. Dithionite was titrated into the prepared OleT under anaerobic conditions while monitored via optical spectroscopy.

Multiple Turnover Activity

OleT (5 μM) was incubated with 500 μM fatty acid substrate (solubilized in 70% ethanol:30% Triton X-100) in 200 mM K_2HPO_4 (pH 7.5). Reactions were initiated by syringe injection of 1000 molar equivalents of H_2O_2 in the same buffer over the course of one hour while stirring. 1-hexadecene (100 nmol) was added as an internal standard and the reaction was quenched with 12 M HCl. The reactions were extracted with equivalent volumes of chloroform and the organic phases pooled and concentrated to 50-100 μL under a stream of N_2. Samples were derivatized with BSTFA:TMCS, sealed, and incubated in a water bath at 60 °C for 20 minutes. The samples were analyzed via gas chromatography mass spectrometry. This methodology remained the same for each heme derivative.

Transient Kinetics

Transient kinetics were determined using an Applied Photophysics Ltd. SX20 stopped-flow spectrophotometer. Three molar equivalents protiated or perdeuterated EA were incubated with 30 μM OleT to form enzyme-substrate (E-S) complexes. The E-S complex was rapidly mixed with 500 molar equivalents of H_2O_2 in 200 mM K_2HPO_4 (pH 7.5). Data was collected using either a photodiode array (PDA) or a photomultiplier tube (PMT) for either full spectral analysis or rate constant determination, respectively. Rate constant determination for Ole-I and Ole-II decay followed that described in previous work[5, 6]. Ole-I and Ole-II decay rate constants were determined for OleT-PP by fitting the time-courses at 690 nm and 440 nm to single and double exponential expressions using ProData viewer. Ole-II decay rates were determined at 440 nm, as this was determined to be where the best accumulation and decay of Ole-II was visible. Utilizing ProData software, Ole-II rates were determined using the following two-sum exponential expression[21]:

$$A_{t,obs} = A_\infty + a_1 e^{-t/t_1} + a_2 e^{-t/t_2}$$

Ole-I decay rates were monitored at 690 nm, and the rates can adequately be fit to single exponential expressions as it is the only contributing species that absorbs at this wavelength [6]. This methodology was also used for OleT-MP and OleT-DP; however, the wavelengths used for Ole-I and Ole-II fitting were 684 nm and 430 nm, and 680 and 435 nm, for MP and DP respectively.

Thermodynamic Studies

Thermodynamic parameters on OleT ferryl intermediates were determined for Ole-I and Ole-II decay rates. The decay rate of these intermediates with protiated and perdeuterated EA was measured using rapid-mix stopped-flow spectroscopy at temperatures ranging from 4 °C to 25 °C.

The rates were fit to an Arrhenius plot (ln$k$ vs. 1/T), providing the activation energy (E_a), derived from the slope of the plot. Fitting the data to an Eyring plot (ln (k/T) vs. 1/T) instead provides $\Delta H^{\ddagger}$ from the slope, and $\Delta S^{\ddagger}$ from the intercept, which is equal to 23.76 + $\Delta S^{\ddagger}/R$ (in J/mol). This methodology remained the same for OleT-MP and OleT-DP, however the wavelengths fit for Ole-I and Ole-II were shifted accordingly.

Reduction Potential Measurements

The reduction potential for OleT was determined spectrophotometrically using a previously described dye/mediator approach[25]. Safranin T (E° = -290 mV) was chosen as a redox indicator dye for OleT-PP and OleT-DP. Neutral Red (E° = -330 mV) was chosen as a redox indicator dye for OleT-MP. A 1 mL mixture of 10 μM OleT and 10 μM dye in 200 mM K_2HPO_4 (pH 7.5) was purged in N_2 gas in a septum-sealed glass bottle for 20 minutes while stirring on ice. The mixture was transferred to an anaerobic cuvette. After initial spectra were taken, anaerobic dithionite was titrated into the cuvette from a stock between 3 and 5 mM in 1 μL aliquots. After each addition, multiple spectra were recorded to ensure equilibrium. This was repeated until both the dye and OleT were fully reduced. Absorbance was recorded at the wavelengths for reduction of LS-OleT and the reduction of the indicator dye. LS-OleT was reduced at 418 nm, 408 nm, and 409 nm for OleT-PP, OleT-MP, and OleT-DP respectively. Safranin T mediator dye was reduced at 525 nm and Neutral Red mediator dye was reduced at 450 nm. Data was processed utilizing the Nernst equation.

$$E_D = E'_{oD} + \frac{RT}{nF}\ln\left[\frac{f_D^o}{f_D^r}\right] = E_P = E'_{oP} + \frac{RT}{nF}\ln\left[\frac{f_P^o}{f_P^r}\right]$$

Utilizing Microsoft Excel, the absorbance was adjusted for the appropriate dilution factor and (mV vs. $\ln(OleT_{Ox}/OleT_{Red})$) was plotted as determined by the Nernst equation. This allows for E_P to be calculated[25]. This methodology remained the same for OleT-PP, OleT-MP, and OleT-DP.

RESULTS AND DISCUSSION

Expression and Purification

Based on the success observed with other heme proteins[26, 27] the heme transporter ChuA was used to incorporate both Fe-mesoporphyrin IX and Fe-deuteroporphyrin IX. For calibration, OleT with Fe-protoporphyrin IX, the native heme, was also expressed with ChuA. Supplementation of modified M9 minimal media with the desired porphyrin and metal during growth allowed for control over the hemes integrated into the protein during growth, as M9 media is not supplemented with other trace metals and has a low hemin content. This forces OleT expressed in *E. coli* grown in M9 media to uptake the iron-porphyrin that is supplemented exogenously.

All three OleT heme analogs were purified via Ni-NTA and butyl-Sepharose columns, yielding approximately 30 mg protein per L of culture, typical of P450 growths[26]. Utilizing both columns ensured the protein was as homogeneous as possible, which was checked using the R_Z ratio. The R_Z value for OleT is determined by A_{418}/A_{280} and should be as close to 1.6 as possible [28]. to limit discrepancies in results that may come from other proteins or contaminants being present in the samples.

Heme Incorporation

Heme incorporation of Fe-mesoporphyrin IX and Fe-deuteroporphyrin IX was successful as confirmed via UV-Vis spectroscopy and liquid chromatography-mass spectrometry (LC-MS) (data not shown). Fe-mesoporphyrin IX incorporation was confirmed through an approximately 15 nm blueshift in the optical spectra, while Fe-deuteroporphyrin IX was suggested through an approximately 8 nm blueshift in the optical spectra. LC-MS chromatograms of heme-extracted

proteins confirmed that OleT-MP and OleT-DP did not contain detectable Fe-protoporphyrin IX, and contained over 90% of the desired porphyrin, confirming successful incorporation via ChuA.

Optical Features

The optical spectra of OleT reconstituted with both Fe-mesoporphyrin IX (OleT-MP) and Fe-deuteroporphyrin IX (OleT-DP), as compared to OleT with the native Fe-protoporphyrin IX (OleT-PP), are shown in Figure 1. The spectra are of the as-purified enzyme in the ferric low-spin (LS) and high-spin (HS) substrate-bound state, as well as the ferrous-CO bound forms following reduction and exposure to CO gas. The previously reported values for each form for OleT-PP were 418 nm for LS, 394 nm for HS, and 446 nm for Fe^{2+}-CO[5, 6]. Substrate binding titrations done with each heme variant probed the retention of the protein environment after cofactor substitution. These binding titrations were used to confirm that global binding of the native substrate was not altered upon heme substitution. Representative binding titrations for OleT-MP, OleT-DP, and OleT-PP with EA are shown in Figure 2. The previously reported K_D for OleT-PP was ~ 300 nM[5], and necessitates fitting to a Morrison equation due to the high-affinity which obviates the free ligand assumption.

Optical Spectroscopic and Binding Characteristics of OleT-MP

In the optical spectrum of OleT-MP, each form is observed to exhibit an approximately 15 nm blue-shift of the Soret maximum relative to that observed for OleT-PP. The new LS-MP maxima is 408 nm, the HS-MP maxima is 382 nm, and the Fe^{2+}-CO-MP maxima is 435 nm. Substrate binding of EA under saturating conditions was fit to a Morrison equation at 382 nm and 408 nm, based on the previously observed optical shifts. The HS state was observed to accumulate to approximately 85% HS at 25 °C, slightly lower than OleT-PP, which has been observed to

accumulate approximate 90% HS [28, 29]. After fitting, the K_D ~ 0.1 μM, which is comparable to that measured for OleT-PP.

Optical Spectroscopic and Binding Characteristics of OleT-DP

In the optical spectrum for OleT-DP, each form is observed to exhibit an approximately 8 nm blue-shift of the Soret maximum relative to that observed for OleT-PP. The new LS-DP maximum is 410 nm, the HS-MP maximum is 387 nm, and the Fe^{2+}-CO-DP maximum is 438 nm. Substrate binding of EA was fit to a Morrison equation at 387 nm and 418 nm. The HS state was observed to accumulate to approximately 75% HS at 25 °C. After fitting, a K_D ~ 3 μM was determined, which is somewhat higher than that measured for OleT-PP.

Conclusions from Optical Binding Studies

Using both the observed, as-purified spectra and the substrate binding parameters, the optical characterization was successful in demonstrating the thiolate ligand and substrate binding pocket remained intact throughout heme substitution for both OleT-MP and OleT-DP. If the substrate binding pocket or thiolate ligand were no longer properly retained, the binding titrations would not be successful. The protein viability is further verified through kinetic experiments and metabolism studies outlined below. The blue-shifted maxima observed for OleT-MP and OleT-DP were consistent for with those observed in other systems[15, 30]. Maxima shift observations additionally allows for indirect heme incorporation confirmation.

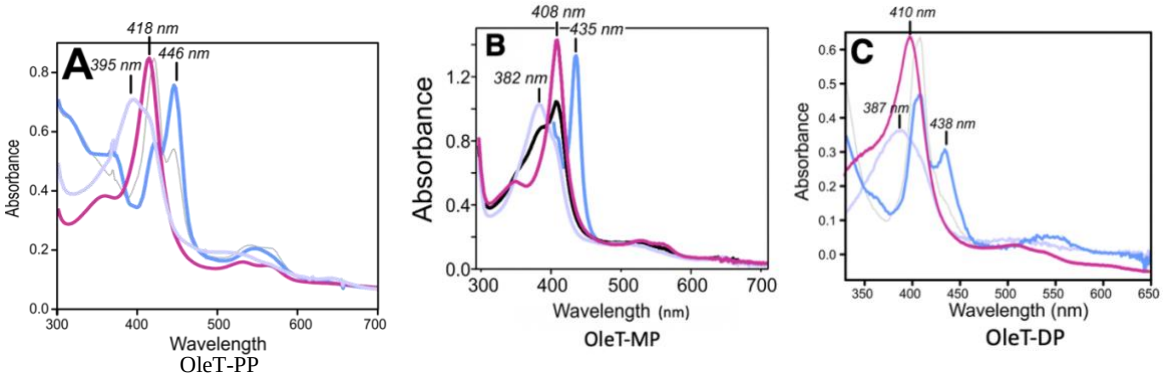

Figure 1: A. The optical spectrum of 10 μM OleT-PP containing adventitiously bound EA low-spin (purple), high-spin (pink), and ferrous CO-bound (blue). Decayed OleT-PP is shown in grey. **B.** The optical spectrum of 10 μM OleT-MP containing adventitiously bound EA low-spin (purple), high-spin (pink), and ferrous CO-bound (blue). The optical spectrum of as-isolated, adventitiously bound EA is shown in black. **C.** The optical spectrum of 10 μM OleT-DP containing adventitiously bound EA low-spin (purple), high-spin (pink), and ferrous CO-bound (blue). Decayed OleT-DP is shown in grey.

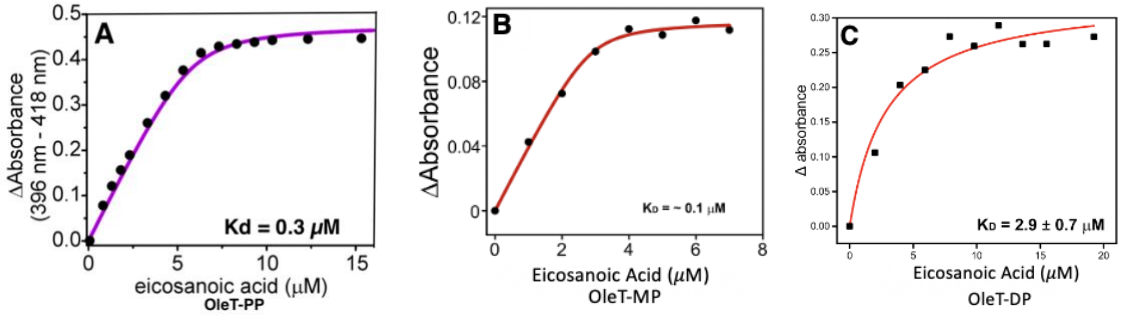

Figure 2: A. The titration of low-spin OleT-PP eicosanoic acid converts the enzyme to the high-spin state, as fit through the Morrison equation[5] (figure modified from Grant et al., 2015). **B.** The titration of low-spin OleT-MP eicosanoic acid converts the enzyme to the high-spin state, as fit through the Morrison equation. **C.** The titration of low-spin OleT-DP eicosanoic acid converts the enzyme to the high-spin state, as fit through the Morrison equation. It should be noted that, although the titration of OleT-PP is given in fraction substrate bound, and OleT-MP and OleT-DP are given in change in absorbance, the K_D values are comparable.

Transient Kinetic Characterization

Prior to this study, the relationship between porphyrin substitution, which alters the $Fe^{3+/}Fe^{2+}$ redox potential and thus potentially ferryl intermediate reactivity has been largely limited to histidine-ligated heme enzymes[16, 31-33]. Unlike OleT, these enzymes do not easily cleave unactivated C-H bonds, such as the C3-H fatty acid abstraction performed by OleT. Moreover, other studies involving substitution of the metal and heme cofactor of P450 enzymes have been unable to investigate Compounds I and II individually. This is due to rate-limiting electron transfer steps that prohibits the ability to directly observe these species for O_2-activating CYPs. The ability to readily observe these two intermediates in OleT offers an opportunity for thermodynamic analysis that has not been done prior to this study.

To investigate OleT ferryl reactivity, stopped-flow spectroscopy was utilized to rapidly mix protiated EA-h_{39}- or deuterated EA-d_{39}-bound reconstituted OleT with 1000 mol. equivalents of H_2O_2. The photodiode array spectra obtained from mixing EA-h_{39}-bound OleT (Figure 3) show Soret maxima at 370 nm for OleT-PP, 360 nm for OleT-MP and 365 nm for OleT-DP. The wavelength shifts are mimicked in the ferric and ferrous spectra, linking the effects of heme substitution between the two electron-conformations. The characteristic π-cation radical signature is also shifted, as it is typically found at 690 nm for OleT-PP. Ole-I accumulation is maintained for both reconstituted enzymes, observed at 690 nm for OleT-PP (Figure 4), allowing them to be used as models to study electronic factors.

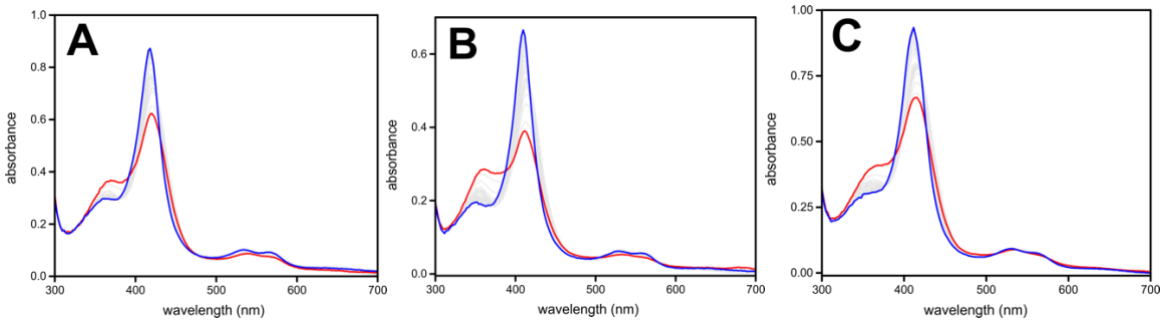

Figure 3: The initial 2 ms trace is shown in red and the final spectrum is shown in blue.

A. Rapid mixing of OleT-PP bound with EA-h_{39} with 1000 molar equivalents of H_2O_2. **B.** Rapid mixing of OleT-MP bound with EA-h_{39} with 1000 molar equivalents of H_2O_2. **C.** Rapid mixing of OleT-DP bound with EA-h_{39} with 1000 molar equivalents of H_2O_2.

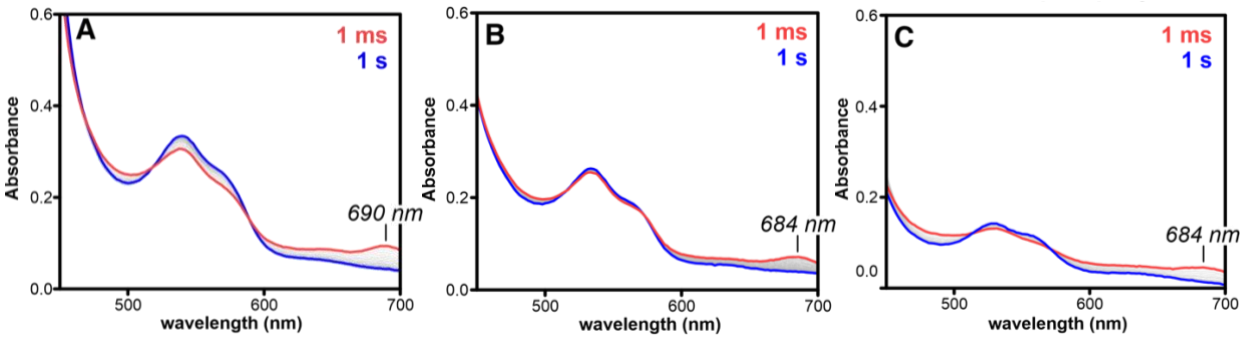

Figure 4: The initial 1 ms trace is shown in red and the final spectrum is shown in blue. **A.** Rapid mixing of OleT-PP bound with EA-d_{39} with 1000 molar equivalents of H_2O_2. **B.** Rapid mixing of OleT-MP bound with EA-d_{39} with 1000 molar equivalents of H_2O_2. **C.** Rapid mixing of OleT-DP bound with EA-d_{39} with 1000 molar equivalents of H_2O_2.

Ole-I and Ole-II Reactivity

To investigate the role of heme substitution on the reactivity of Ole-I and Ole-II, single wavelength data was collected using a photomultiplier tube (PMT) to determine individual rate constants, as shown in Table 1. For OleT-PP, Ole-I and Ole-II decay rates were 25 ± 1 s^{-1} and 14.4 ± 0.1 s^{-1} at 277 K, respectively. k_2 = 9.7 ± 0.1 s^{-1}

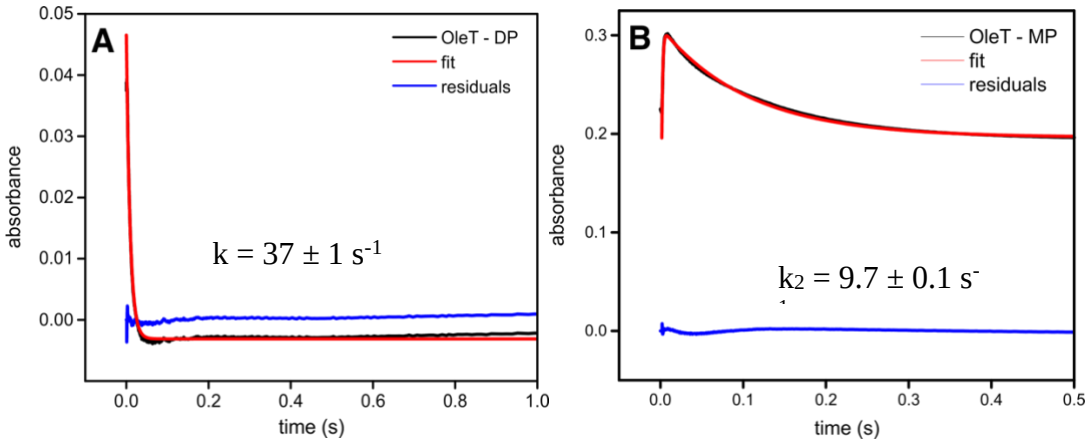

Figure 5: A. Compound I decay of OleT-MP as measured at 684 nm is fit with a single exponential equation. **B.** Compound II formation and decay of OleT-MP as measured at 435 nm is fit with a two-summed exponential expression.

OleT-MP: Compound-I decay, as measured at 684 nm when OleT-MP was EA-d_{39}-bound, was fit to a single exponential equation to determine the rate constant. Single exponential fitting reflects a homogenous process, meaning there is a single step to the reaction. OleT-MP-I decay was measured to be 37 ± 1 s^{-1} at 4 °C (Figure 5). OleT-MP-I accumulation significantly decreased upon the reaction with EA-h_{39}, as the decay rate is significantly accelerated to over 700 s^{-1}, which approaches the limits of the instrument for accurate rate constant determination. Compared to OleT-PP, OleT-MP exhibits an approximately 50% faster C-D Ole-I decay rate as compared to OleT-PP-I. This is as expected from a more electron-rich heme, and there may be more stability in the O-H/D bond, which as has been observed in other hydrogen abstracting enzymes[34].

Compound-II decay was measured for OleT-MP at 430 nm (Figure 5), which is the maximum change in absorbance between OleT-MP-II and LS at 408 nm. The rate of OleT-MP-II decay can be fit to a double exponential equation, with a formation rate of 700 ± 30 s^{-1} and a decay rate of 9.7 ± 0.1 s^{-1} when OleT-MP was EA-h_{39} bound. The formation rate of 700 ± 30 s^{-1} matches

that of OleT-MP-I decay, which is expected. OleT-MP-II decay is about 33% slower than OleT-PP-II decay, indicating a weakened oxidizing potential.

Table 1: Compound I and Compound II decay rates as measured at 4 °C for OleT-PP, OleT-MP, and OleT-DP.

	Deuterated Decay Rates		**Protiated Decay Rates**	**^{2}H KIE**	**Reference**
	Ole-I (s^{-1})	*Ole-II (s^{-1})*	*Ole-I (s^{-1})*	*Ole-I KIE*	
PP	~ 80 **(370 nm)**	~ 10.8	~ 300	>8	*5, 6*
PP	25 ± 1 **(690 nm)**	14.4 ± 0.1	>700	18.12 ± 0.06	*This work*
MP	37 ± 1	9.7 ± 0.1	>700	4.68 ± 0.05	*This work*
DP	111 ± 5	17.2 ± 0.3	>700	11.04 ± 0.09	*This work*

OleT-DP: Compound-I decay, as measured at 685 nm when OleT-DP was EA-d_{39}-bound, required fitting to a single exponential to determine the rate. OleT-DP-I decay was measured to be 111 ± 5 s^{-1} at 4 °C (Figure 6). OleT-DP-I accumulation significantly decreased upon binding with EA-h_{39}, as the decay rate is significantly accelerated to over 700 s^{-1}, which is at the limits of the instrument. Compared to OleT-PP-I, OleT-DP-I is observed to abstract C-D approximately five times faster.

Compound-II decay was measured for OleT-DP at 435 nm (Figure 6), which is the maximum difference in absorbance between OleT-DP-II and the LS enzyme. The rate of OleT-DP-II decay can be fit to a double exponential equation, with a formation rate of 700 ± 30 s^{-1} and a decay rate of 17.2 ± 0.3 s^{-1} when OleT-DP was EA-h_{39} bound. The formation rate of 700 ± 30 s^{-1} matches that of OleT-DP-I decay, which is expected. OleT-DP-II decay rate is slightly faster than OleT-PP-II, indicating a similar or slightly better oxidizing potential.

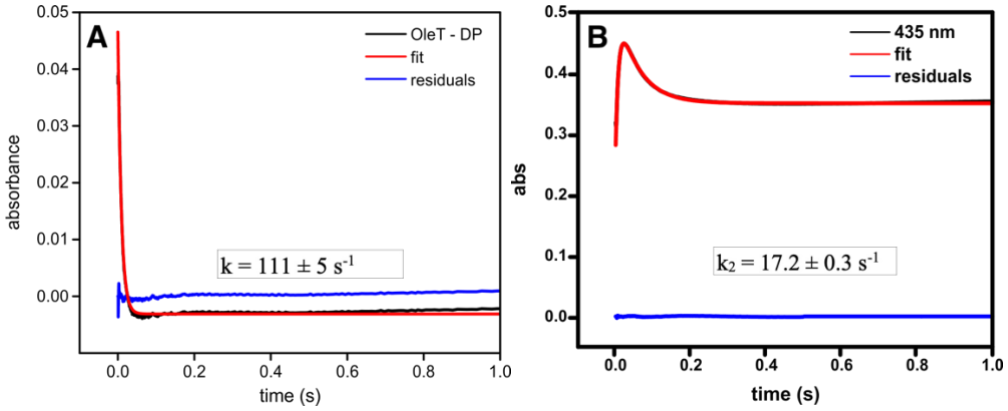

Figure 6: A. Compound I decay of OleT-DP as measured at 685 nm is fit with a single exponential equation. **B.** Compound I formation and Compound II decay of OleT-DP as measured at 435 nm is fit with a double exponential equation.

Kinetic Isotope Effect: The kinetic isotope effect (KIE) for Ole-I varies greatly between the three porphyrin substituents. This is particularly clear between OleT-PP-I and OleT-MP-I, with the KIE for OleT-MP-I being almost four times smaller than that of OleT-PP-I. The significantly smaller KIE may be indicative of a different rate determining step[35]. It is possible that the alterations in the porphyrin are affecting the peroxide activation or hydrogen abstraction in a way that perturbs the traditional catalytic cycle [6].

Activation Thermodynamics

Ole-I: In order to differentiate the effects of the various porphyrin substituents on the first-order C-H abstraction rate by Compound-I, a temperature dependence study was done on Ole-I to measure decay rates from 4 °C to 25 °C when OleT was bound to EA-d_{39}. OleT bound to EA-h_{39} was attempted, however the rates of Ole-I decomposition become unreliably fast at elevated temperatures. Nonetheless, utilizing deuterium-bound substrate allows for the comparison between porphyrin parameters, as rates remained within the detection limits of the equipment.

Throughout the temperature-dependence studies, there was approximately a 3-fold rate change observed over the temperature range probed for each porphyrin. Arrhenius behavior was observed, with no breaks in the Arrhenius plot. This indicates a uniform reaction coordinate (e.g., consistent rate limiting step) across the temperature range. Fitting to an Eyring Plot (ln(k/T) vs (1/T)) (Figure 7), the thermodynamic parameters of Ole-I can be determined and are listed in Table 2. Compared to OleT-PP-I, Ole-I decay by OleT-MP-I is less endothermic but exhibits a larger entropic penalty. The magnitude of $\Delta G^{\ddagger}$ is significantly lowered for OleT-MP-I as well. OleT-DP-I has similar enthalpic and entropic values to OleT-MP-I, leading to a similar $\Delta G^{\ddagger}$, which is much also much lower than that of OleT-PP-I. OleT-MP-I and OleT-DP-I have somewhat similar activation energies, which are both significantly lower than that for OleT-PP-I. The activation energy for OleT-DP-I is higher than that for OleT-MP-I, by almost 1 kcal/mol. This is likely due to their differences in entropy, as they have very relatively similar enthalpic values. All three OleT porphyrin homologs have relatively similar enthalpic values for the Ole-I reaction and are within 1.5 kcal/mol of each other. There is a significant difference in the Gibbs free energy, however, which is from the entropic differences between the three porphyrin variants. This entropically-driven variation in porphyrin-thermodynamics can be observed in other metalloproteins[36]

Ole-II: Similar studies were done to determine whether the effect seen with Ole-I was also seen with Ole-II. OleT was bound to EA-h_{39}. Similar to Ole-I, Arrhenius dependence was observed with Ole-II, with no breaks in the Arrhenius plot. Fitting to an Eyring Plot (ln(k/T) vs (1/T)) (Figure 7), the thermodynamic parameters of Ole-II can be determined and are listed in Table 2. Compared to OleT-PP-II, OleT-MP-II has somewhat similar enthalpic values, and similar entropic values, leading to fairly similar values of $\Delta G^{\ddagger}$. The activation barrier is higher for OleT-MP-II than it is

for OleT-PP-I, which may be due to increased enthalpic penalties. Taken together, both native and non-native porphyrin analogs have lower activation barriers for Ole-II as compared to Ole-I.

Compared to Ole-I, it appears as though enthalpy may play a larger role as compared to entropy in Ole-II reactivity. As greater changes are seen with different porphyrin derivatives in enthalpy, and there is a greater enthalpic penalty for OleT-MP-II to yield a larger activation barrier, this may be the case; however, further studies with other porphyrin derivatives would be necessary to confirm this as OleT-DP could not be analyzed in this study.

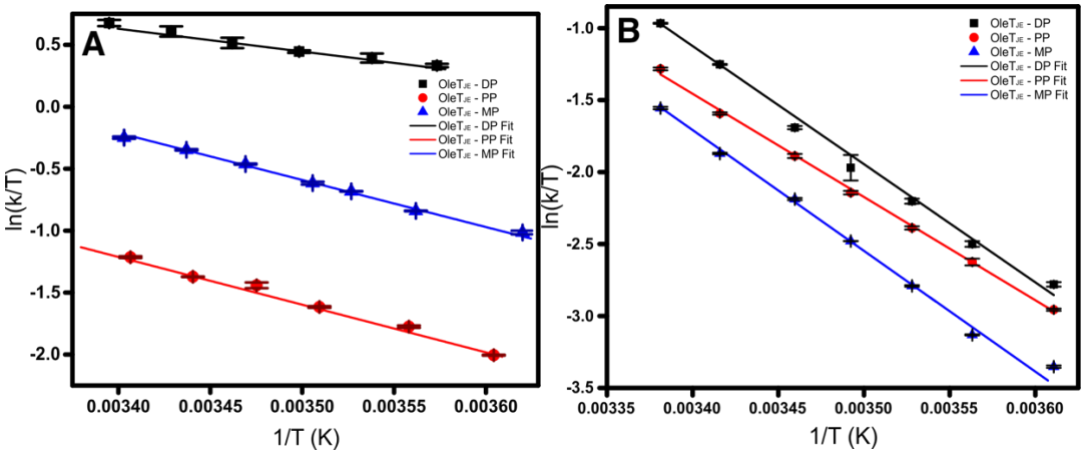

Figure 7: A. Eyring plot of Compound I decay for all three porphyrin derivatives. OleT-PP is shown in red, OleT-MP is shown in blue, and OleT-DP is shown in black. Rates were determined through averaging at least three measurements at each temperature, and error bars represent one standard deviation. **B.** Eyring plot of Compound II decay for all three porphyrin derivatives. OleT-PP is shown in red, OleT-MP is shown in blue, and OleT-DP is shown in black. Rates were determined through averaging at least three measurements at each temperature, and error bars represent one standard deviation.

Table 2: Activation thermodynamic parameters as determined from the Eyring plots in Figure 7 of the Ole-I decay rates. $\Delta G^{\ddagger}$ is determined at a temperature of 25 °C (298 K).

	PPIX-OleT$_{JE}$		**Meso-OleT$_{JE}$**		**Deutero-OleT$_{JE}$**	
Parameter	**C20D-FA**	**C20H-FA**	**C20D-FA**	**C20H-FA**	**C20D-FA**	**C20H-FA**
ΔH (kcal/mol)	8.95±0.09	5.50±0.97	7.57±0.12	6.36±0.75	7.25±0.13	--
ΔS (cal/mol)	-19.72±0.19	-24.62±3.48	-23.86±0.55	-22.27±3.12	-23.03±0.35	--
ΔG (kcal/mol)	14.83±0.33	12.84±1.38	9.27±0.17	13.00±0.75	8.89±0.42	--
Ea (kcal/mol)	9.55±0.06	6.09±1.8	6.97±0.30	6.95±2.1	7.84±0.39	--

Redox Potential

Based on previous studies, reducing the heme side groups is hypothesized to shift to lower heme reduction potential[37, 38]. The measured potential of substrate-free OleT-PP, using a dye-mediator approach, indicated a midpoint redox potential of -300 ± 16 mV, as shown by the Nernst plot (Figure 8).

The redox potential of substrate-free OleT-MP was measured through spectroelectrochemical methods using a dye-mediator approach. Incorporating OleT-MP led to a significant decrease in redox potential, with a midpoint potential measured to be -340 ± 18 mV (Figure 8). This decrease in redox potential is consistent with what has been observed in other heme proteins undergoing MP substitution[15]. The redox potential of substrate-free OleT-DP was measured through spectroelectrochemical methods using a dye-mediator approach. Incorporating OleT-DP led to a

slight decrease in redox potential, with a midpoint potential measured to be -310 ± 10 mV (Figure 8). This decrease in redox potential was as hypothesized, to be in between PP and MP.

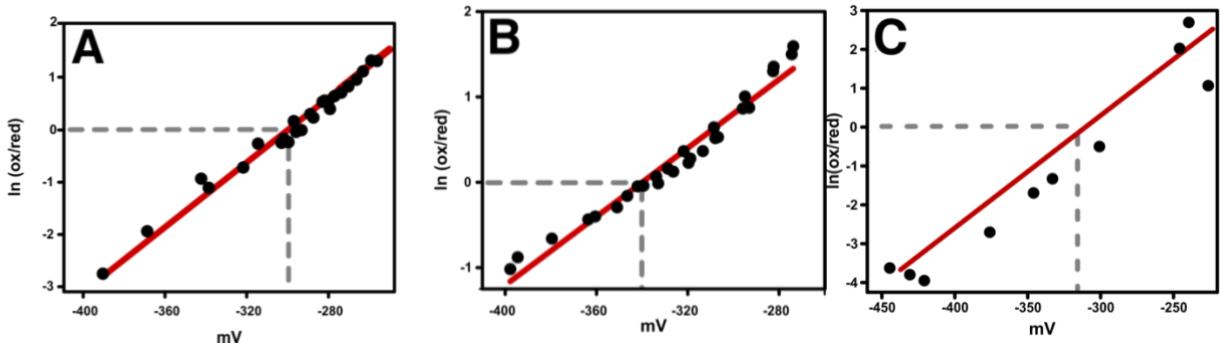

Figure 8: The Nernst plots for the reduction potentials of **A.** OleT-PP in the presence of Safranin T mediator dye; **B.** OleT-MP in the presence of Neutral Red mediator dye; and **C.** OleT-DP in the presence of Safranin T mediator dye.

Several factors can impact the reduction potential of cytochromes, including the electrostatic charge on the ligand, the donor power of the ligand, the acceptor power of the ligand, changes in metal ion spin state, and steric factors [38]. Axial ligands have been observed to have a dominant effect over reduction power[38]; however, in this scenario the heme retains the same ligand and surrounding microenvironment in each porphyrin substituent.

Instead, using pK_3 values, which impact the donor power of the heme[38], the redox potentials reported in this work follow trends previously reported for the porphyrin isomers and their pK_3 values[23, 37]. MP was reported to have the greatest pK_3 value[23, 37], and has been observed to have the most negative reduction potential, while PP was reported to have the smallest pK_3 value[23, 37], and has been observed to have the least negative reduction potential.

Conclusions

Through the successful *in vivo* incorporation of MP and DP into OleT, this work explores the impact of altering reduction potential on thermodynamic properties. For the first time, the

direct measurement of the influence of ground-state thermodynamics on C-H abstraction by P450 Compound has been explored, as well as how these effects alter Compound I and II reactivity.

Electron Density: One proposed reason for this alteration in reactivity is due to differences in electron density surrounding the Fe. MP has greater electron density as compared to PP; thus, this substitution leads to a -40 mV shift in the $Fe^{2+/3+}$ redox potential of OleT. The substitution from PP to MP results in a moderate change in acceleration rate, with OleT-MP being faster that OleT-PP. Alternatively, DP has less electron density surrounding the Fe as compared to both MP and PP, but this substitution leads to a -10 mV shift in the $Fe^{2+/3+}$ redox potential. The substitution of OleT-DP resulted in a much greater change in acceleration rate, being faster than both OleT-MP and OleT-PP. If the alteration in Compound I reactivity was due to electron density around the Fe, then the trend in reduction potential would need to follow the electron density or vice versa.

Bond Strength: Another, more likely, proposed reason for the alteration in reactivity is due to alterations in C – H bond strength with the different porphyrin substitutions. Based on the methods to calculate C – H bond strength by Mittra & Green (2019) C – H bond strength is both pKa and E^0 dependent. The energy to break the D-OH bond remains fairly constant for each porphyrin substitution (Table 3); however, with changes in pKa, there are significant changes in the energy needed to break the D(C – H) bond. The increase in pKa leads to a lower energy necessary to break the bond, with OleT-DP requiring the least amount of energy (Table 3). This is consistent with the reactivity results, as OleT-DP also had the fastest C – H abstraction based on Ole-I and Ole-II reactivity. Based on these two proposed mechanisms, it is much more likely that the changes in reactivity are based on differences in pKa resulting from the porphyrin substitutions. The higher pKa may make hydrogen abstraction easier.

Porphyrin pK_3 values are observed to have a negative linear relationship with activation energy (Figure 9). As the pK_3 value of the porphyrin increases, the activation energy of Ole-I decreases for each porphyrin substituent. Based on previous literature to lower the activation energy of CYP enzymes through modifications to the iron-cysteine thiolate ligation to increase pK_a [20], this relationship is not unexpected but interesting nonetheless and supports the bond energy theory.

Table 3: Calculated bond strengths based off of pK_3[37] for OleT-PP, OleT-MP, and OleT-DP.

	pK_3 [23, 37]	**ΔG** (kcal/mol)	**D-OH** (kcal/mol)	**D(C-H)** (kcal/mol)
OleT-PP	4.8	14.8	57.3	72.1
OleT-MP	5.8	9.3	57.7	67.0
OleT-DP	5.5	8.9	58.0	66.8

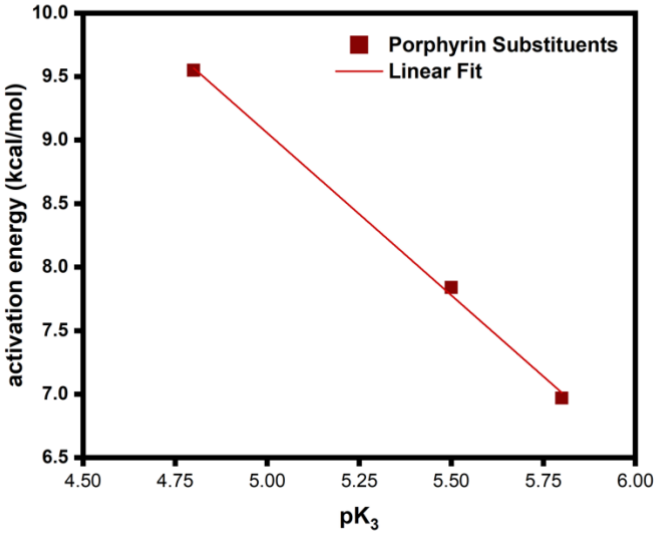

Figure 9: The observed pK_3 versus the calculated activation energy in kcal/mol for each porphyrin substituent. There is a clear, negative linear relationship between the two parameters.

Porphyrin modification appears to significantly lower the activation barrier to hydrogen abstraction by Compound I. This phenomenon appears to be based in entropy, as the enthalpic factor remains fairly constant throughout the porphyrin modifications (Table 2). The entropic factor undergoes the most change to result in the lowering of the free energy and the activation barrier to produce the results reported here.

Future Directions

At this point, more studies are needed to further confirm the results of this work. Additional porphyrins should be incorporated into OleT, particularly porphyrins that would shift the reduction potential in the opposite direction. This would confirm the trends observed here. Additionally, it would be beneficial to develop a method to directly measure the pH and influence of pH on porphyrin thermodynamics. The proposed pKa mechanism here should be confirmed, however the method for this needs to be developed.

REFERENCES

1. Hill, J.; Nelson, E.; Tilman, D.; Polasky, S.; Tiffany, D., Environmental, economic, and energetic costs and benefits of biodiesel and ethanol biofuels. *Proceedings of the National Academy of Sciences* **2006,** *103* (30), 11206-11210.

2. Wise, C. E.; Grant, J. L.; Amaya, J. A.; Ratigan, S. C.; Hsieh, C. H.; Manley, O. M.; Makris, T. M., Divergent mechanisms of iron-containing enzymes for hydrocarbon biosynthesis. *JBIC Journal of Biological Inorganic Chemistry* **2017,** *22* (2-3), 221-235.

3. Rude, M. A.; Baron, T. S.; Brubaker, S.; Alibhai, M.; Del Cardayre, S. B.; Schirmer, A., Terminal Olefin (1-Alkene) Biosynthesis by a Novel P450 Fatty Acid Decarboxylase from Jeotgalicoccus Species. *Applied and Environmental Microbiology* **2011,** *77* (5), 1718-1727.

4. Munro, A. W.; McLean, K. J.; Grant, J. L.; Makris, T. M., Structure and function of the cytochrome P450 peroxygenase enzymes. *Biochemical Society Transactions* **2018,** *46* (1), 183-196.

5. Grant, J. L.; Hsieh, C. H.; Makris, T. M., Decarboxylation of Fatty Acids to Terminal Alkenes by Cytochrome P450 Compound I. *Journal of the American Chemical Society* **2015,** *137* (15), 4940-4943.

6. Grant, J. L.; Mitchell, M. E.; Makris, T. M., Catalytic strategy for carbon−carbon bond scission by the cytochrome P450 OleT. *Proceedings of the National Academy of Sciences* **2016,** *113* (36), 10049-10054.

7. Belcher, J.; McLean, K. J.; Matthews, S.; Woodward, L. S.; Fisher, K.; Rigby, S. E.; Nelson, D. R.; Potts, D.; Baynham, M. T.; Parker, D. A., Structure and biochemical properties of the alkene producing cytochrome P450 OleTJE (CYP152L1) from the Jeotgalicoccus sp. 8456 bacterium. *Journal of Biological Chemistry* **2014,** *289* (10), 6535-6550.

8. Matthews, S.; Tee, K. L.; Rattray, N. J.; McLean, K. J.; Leys, D.; Parker, D. A.; Blankley, R. T.; Munro, A. W., Production of alkenes and novel secondary products by P450 OleTJE using novel H2O2-generating fusion protein systems. *FEBS Letters* **2017,** *591* (5), 737-750.

9. Li, F.; Yang, K.; Xu, Y.; Qiao, Y.; Yan, Y.; Yan, J., A genetically-encoded synthetic self-assembled multienzyme complex of lipase and P450 fatty acid decarboxylase for efficient bioproduction of fatty alkenes. *Bioresource technology* **2019,** *272*, 451-457.

10. Daff, S.; Chapman, S. K.; Turner, K.; Holt, R.; Govindaraj, S.; Poulos, T.; Munro, A., Redox control of the catalytic cycle of flavocytochrome P-450 BM3. *Biochemistry* **1997,** *36* (45), 13816-13823.

11. Funk, W. D.; Lo, T. P.; Mauk, M. R.; Brayer, G. D.; MacGillivray, R. T.; Mauk, A. G., Mutagenic, electrochemical, and crystallographic investigation of the cytochrome b5 oxidation-reduction equilibrium: involvement of asparagine-57, serine-64, and heme propionate-7. *Biochemistry* **1990,** *29* (23), 5500-5508.

12. Munro, A. W.; Girvan, H. M.; McLean, K. J., Cytochrome P450–redox partner fusion enzymes. *Biochimica et Biophysica Acta (BBA) - General Subjects* **2007,** *1770* (3), 345-359.

13. Mittra, K.; Green, M. T., Reduction Potentials of P450 Compounds I and II: Insight into the Thermodynamics of C–H Bond Activation. *Journal of the American Chemical Society* **2019,** *141* (13), 5504-5510.

14. Hsieh, C. H.; Huang, X.; Amaya, J. A.; Rutland, C. D.; Keys, C. L.; Groves, J. T.; Austin, R. N.; Makris, T. M., The Enigmatic P450 Decarboxylase OleT Is Capable of, but Evolved To Frustrate, Oxygen Rebound Chemistry. *Biochemistry* **2017,** *56* (26), 3347-3357.

15. Tejero, J.; Biswas, A.; Haque, M. M.; Wang, Z.-Q.; Hemann, C.; Varnado, C. L.; Novince, Z.; Hille, R.; Goodwin, D. C.; Stuehr, D. J., Mesohaem substitution reveals how haem electronic properties can influence the kinetic and catalytic parameters of neuronal NO synthase. *Biochemical Journal* **2011,** *433* (1), 163-174.

16. Shinohara, A.; Kamataki, T.; Iizuka, T.; Ishimura, Y.; Ogoshi, H.; Okuda, K.; Kato, R., Drug Oxidation Activities of Horseradish Peroxidase, Myoglobin and Cytochrome P-450cam Reconstituted with Synthetic Hemes†. *Japanese Journal of Pharmacology* **1987,** *45* (1), 107-114.

17. Bhagi-Damodaran, A.; Petrik, I. D.; Marshall, N. M.; Robinson, H.; Lu, Y., Systematic Tuning of Heme Redox Potentials and Its Effects on O2 Reduction Rates in a Designed Oxidase in Myoglobin. *Journal of the American Chemical Society* **2014,** *136* (34), 11882-11885.

18. Green, M. T., CH bond activation in heme proteins: the role of thiolate ligation in cytochrome P450. *Current Opinion in Chemical Biology* **2009,** *13* (1), 84-88.

19. Rittle, J.; Green, M. T., Cytochrome P450 Compound I: Capture, Characterization, and C-H Bond Activation Kinetics. *Science* **2010,** *330* (6006), 933-937.

20. Yosca, T. H.; Rittle, J.; Krest, C. M.; Onderko, E. L.; Silakov, A.; Calixto, J. C.; Behan, R. K.; Green, M. T., Iron(IV)hydroxide pK(a) and the role of thiolate ligation in C-H bond activation by cytochrome P450. *Science (New York, N.Y.)* **2013,** *342* (6160), 825-829.

21. Amaya, J. A.; Rutland, C. D.; Leschinsky, N.; Makris, T. M., A Distal Loop Controls Product Release and Chemo- and Regioselectivity in Cytochrome P450 Decarboxylases. *Biochemistry* **2018,** *57* (3), 344-353.

22. Froger, A.; Hall, J. E., Transformation of plasmid DNA into E. coli using the heat shock method. *J Vis Exp* **2007,** (6), 253-253.

23. Dolphin, D.; James, B. R.; Welborn, H. C., Oxygenation, and carbonylation, of a reduced P450cam enzyme and derivatives reconstituted with mesodeutero-, dibromodeutero-, and diacetyldeuteroheme. *Journal of Molecular Catalysis* **1980,** *7* (2), 201-213.

24. Mao, L.; Luo, S.; Huang, Q.; Lu, J., Horseradish Peroxidase Inactivation: Heme Destruction and Influence of Polyethylene Glycol. *Scientific Reports* **2013,** *3* (1), 3126.

25. Sligar, S. G.; Gunsalus, I. C., A thermodynamic model of regulation: modulation of redox equilibria in camphor monoxygenase. *Proceedings of the National Academy of Sciences* **1976,** *73* (4), 1078-1082.

26. Varnado, C. L.; Goodwin, D. C., System for the expression of recombinant hemoproteins in Escherichia coli. *Protein Expression and Purification* **2004,** *35* (1), 76-83.

27. Reynolds, E. W.; Schwochert, T. D.; McHenry, M. W.; Watters, J. W.; Brustad, E. M., Orthogonal expression of an artificial metalloenzyme for abiotic catalysis. *ChemBioChem* **2017,** *18* (24), 2380-2384.

28. Amaya, J. A. Mechanisms Of Decarboxylation In The CYP152
Family Of Cytochrome P450S. Doctoral Dissertation, University of South Carolina, Scholar Commons, 2018.

29. Wise, C. E.; Hsieh, C. H.; Poplin, N. L.; Makris, T. M., Dioxygen Activation by the Biofuel-Generating Cytochrome P450 OleT. *ACS Catalysis* **2018,** *8* (10), 9342-9352.

30. Bender, A. T.; Kamada, Y.; Kleaveland, P. A.; Osawa, Y., Assembly and activation of heme-deficient neuronal NO synthase with various porphyrins. *Journal of Inorganic Biochemistry* **2002,** *91* (4), 625-634.

31. Terner, J.; Palaniappan, V.; Gold, A.; Weiss, R.; Fitzgerald, M. M.; Sullivan, A. M.; Hosten, C. M., Resonance Raman spectroscopy of oxoiron(IV) porphyrin π-cation radical and

oxoiron(IV) hemes in peroxidase intermediates. *Journal of Inorganic Biochemistry* **2006,** *100* (4), 480-501.

32. Groves, J. T.; Boaz, N. C., Fishing for peroxidase protons. *Science* **2014,** *345* (6193), 142-143.

33. Poulos, T. L., Heme enzyme structure and function. *Chem Rev* **2014,** *114* (7), 3919-3962.

34. Wang, K.; Mayer, J. M., Oxidation of Hydrocarbons by [(phen)2Mn(μ-O)2Mn(phen)2]3+ via Hydrogen Atom Abstraction. *Journal of the American Chemical Society* **1997,** *119* (6), 1470-1471.

35. Brazeau, B. J.; Wallar, B. J.; Lipscomb, J. D., Unmasking of Deuterium Kinetic Isotope Effects on the Methane Monooxygenase Compound Q Reaction by Site-Directed Mutagenesis of Component B. *Journal of the American Chemical Society* **2001,** *123* (42), 10421-10422.

36. Sato, F.; Shiro, Y.; Sakaguchi, Y.; Iizuka, T.; Hayashi, H., Thermodynamic study of protein dynamic structure in the oxygen binding reaction of myoglobin. *J Biol Chem* **1990,** *265* (31), 18823-8.

37. Singh, U. P.; Obayashi, E.; Takahashi, S.; Iizuka, T.; Shoun, H.; Shiro, Y., The effects of heme modification on reactivity, ligand binding properties and iron-coordination structures of cytochrome P450nor. *Biochimica et Biophysica Acta (BBA) - Protein Structure and Molecular Enzymology* **1998,** *1384* (1), 103-111.

38. Moore, G. R.; Williams, R. J., Structural basis for the variation in redox potential of cytochromes. *FEBS letters* **1977,** *79* (2), 229-232.